Characterization of Strain-Tolerant Ceramic/SAM Bilayer Coatings

Q. Yang[*], T. O. Salami[†], K. Chitre[*], S. R. Oliver[†], and J. Cho[*]
Dept. of Mechanical Engineering[*]
Dept. of Chemistry[†]
State University of New York, Binghamton

ABSTRACT

Ceramic coatings can provide an ideal protection for MEMS (MicroElectroMechanical Systems) structures while imposing a great challenge in processing a prime, reliant coating due to their inherent brittleness and defects formed during processing. In an attempt to compensate for the weakness of the ceramic coating, we have developed a low-temperature solution precursor process to create strain-tolerant, protective bilayer coating consisting of an integrated ceramic-organic hybrid material. The top ceramic coating offers an inert, protective layer whereas the underlying nanometer scale self-assembled organic coating provides compliance for the overlying hard coating. Together, these bilayers minimize mechanical and thermal stresses. In addition, organic self-assembled monolayers(SAM) act as a 'template' by forming a proper surface functionality for the subsequent growth of hard ceramic coatings. Molecular level understanding of the microstructure and micromechanics involved in the synthesis and processing of the coating is systematically studied by a variety of characterization techniques such as XRD, AFM, SEM/EDS and nanoindentation. This work is also complemented by numerical simulation to provide a clearer understanding of the stress development in the ceramic coating and its interfacial properties.

INTRODUCTION

MEMS have received a great deal of attention because of their promising applications spanning the navigation, automotive, military, and seismic markets [1-3]. However, the cost and reliability issues with MEMS have yet to be optimized. A common issue in MEMS is the need of high-vacuum hermetically sealed packaging to isolate and protect the device against adverse environmental effects. Hermetic packaging, however, not only increases the size of a MEMS device, but it also raises the cost. It is estimated that hermetic packaging is responsible for 70-95% of the overall cost of a MEMS [4,5]. Cost reduction in the fabrication of high-performance and automotive electronic and MEMS devices is indeed a main driving force for their application.

One sensible way to tackle the current limitations imposed on MEMS is to deposit a protective coating layer on the surface of silicon. Protected silicon structures in MEMS may no longer need a hermetic sealing to protect them from environmental effects while providing a protection from a variety of environments. Good candidate materials for surface coatings are ceramics due to their high degree of hardness and modulus. Ceramics have indeed been employed for protective coatings in numerous applications. Particular examples include oxide ceramics such as Al_2O_3 and ZrO_2 as well as non-oxide ceramics such as TiN, TiC, TiAlN, and cubic boron nitride (c-BN) [6-10].

Conventional ceramic processing, however, involves high temperature sintering and cannot be easily implemented for surface coatings. Therefore, a major challenge to produce ceramic

coatings on silicon is to have a low-temperature synthetic route with minimal shrinkage during processing. ZrO_2 is used as our model system in order to have a basic understanding of ceramic film growth on the underlying organic layer. A self-assembly technique is used to grow the organic monolayer on the Si/SiO_2 substrate [11-14]. This self-assembled monolayer (SAM) is used as an organic template to engineer the surface for the ceramic film growth.

We report herein the synthesis of the bilayer coatings with focus on characterization of the coating films. In addition, preliminary construction of numerical modeling for the bilayer structure is presented.

EXPERIMENTAL PROCEDURE

The substrates used in this study are N-doped [100] single crystal silicon wafers (Silicon Quest International, Santa Clara, CA). The silicon was hydrolyzed by exposing to freshly prepared piranha solution (1 H_2O_2:3 H_2SO_4) before deposition.

The organic layer was deposited on the hydrolyzed silicon wafer from trichlorosilane precursor solutions in a vacuum-sealed cell or a glove box. Ceramic deposition was carried out by in-situ solution process (biomimetic) and spin-coating method.

For in-situ solution process, a freshly prepared 0.01-*m* solution of one of two different ceramic precursors (zirconium sulfate ($Zr(SO_4)_2 \cdot 4H_2O$) and zirconyl chloride ($ZrOCl_2 \cdot 8H_2O$), both from Alfa Aesar, Ward Hill, MA) was used. The substrates (SAM-coated silicon wafers or cleaned bare silicon wafers) were submerged in these precursor solutions for 24 hours using a constant temperature oil bath maintained at 80 °C. After 24 hours the wafers were taken out, rinsed with distilled water and dried in a stream of nitrogen

In the spin coating method, bare silicon and SAM deposited wafers were spin coated with freshly prepared precursor solutions (3-*m* zirconyl chloride or zirconium sulfate). The spin-coated wafers were pyrolyzed at elevated temperatures to obtain a zirconium oxide (ZrO_2) film. The deposited films were characterized by x-ray diffraction (XRD), energy-dispersive spectroscopy (EDS), and atomic force microscope (AFM). Mechanical properties of the films, namely elastic modulus and hardness, were measured with a nanoindenter (Hysitron TriboScope, Minneapolis, MN). This instrument is coupled with an *in-situ* imaging capability via AFM. Information obtained from indentation includes reduced elastic modulus E_r and hardness H [15]. Reduced elastic modulus E_r is related with the actual modulus of the film as given by

$$\frac{1}{E_r} = \left(\frac{1-\nu^2}{E}\right)_{sample} + \left(\frac{1-\nu^2}{E}\right)_{indenter}, \qquad (1)$$

where E and ν are the elastic modulus and Poisson's ratio. The modulus of the indenter for our instrument is 1140 GPa, and Poisson's ratio is 0.07.

The hardness H has the normal definition as given by

$$H = \frac{P_{\max}}{A}, \qquad (2)$$

where $P_{\max}$ is the maximum indentation load and A is the resultant projected contact area at that load.

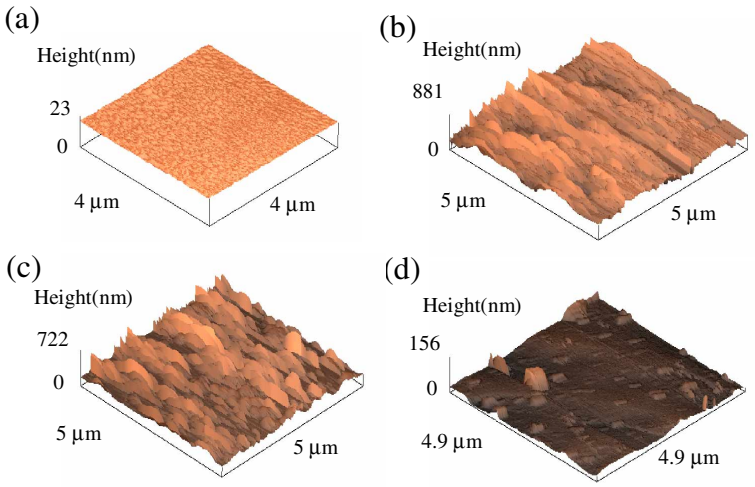

Figure 1. AFM images obtained from the coatings derived from the zirconia precursor solutions: (a) zirconyl chloride on -PO_3H_2-terminated SAM at pH=1.1; (b) same as part (a) except at pH=9.6; (c) zirconium sulfate on -$SiCl_3$-terminated SAM at pH=1.1; (d) same as part (c) except at pH=9.6.

RESULTS AND DISCUSSION

The coating made by the in-situ solution process was affected by numerous factors such as pH value of the solution, substrate condition, and precursor chemistry. As shown in Fig. 1, the coating is not observed when the substrate (Si deposited with -PO_3H_2 teminated SAM) is deposited with the zirconyl chloride precursor in an acidic solution (pH=1.1) while the coating is clearly observed when deposited in a basic solution (pH=9.6). On the other hand, zirconium sulfate precursor produced coating on the substrates (Si deposited with -$SiCl_3$ teminated SAM) in an acidic solution (pH=1.1), but not in a basic solution (pH=9.6).

Characterization was focused on the spin-coated samples prepared using 3-*m* $Zr(SO_4)_2{\cdot}4H_2O$ solution and in-situ prepared samples at 80°C in 0.01-*m* $Zr(SO_4)_2{\cdot}4H_2O$. The substrates for both cases were -PO_3H_2 terminated SAM coated Si. X-ray diffraction results showed that as deposited phase from the spin coating process is a crystalline zirconium sulfate that is maintained until the amorphous phase appears at 500°C (Fig. 2). A raw zirconium sulfate powder reagent (as received) also exhibited the same crystalline phase. For continuous annealing treatments at elevated temperatures, *t*- and *m*-ZrO_2 phases began to appear at ~800°C along with an amorphous phase. These crystalline phases became more dominant at 1000°C.

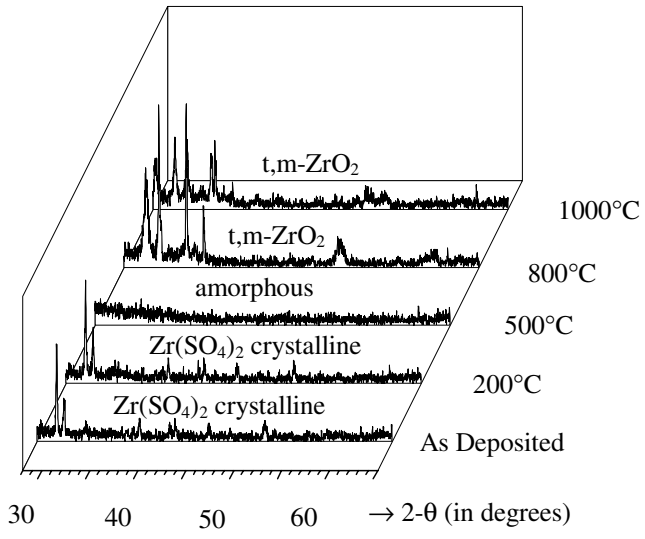

Figure 2. XRD of spin-coated samples prepared using 3-*m* zirconium sulfate solution on -PO_3H_2 terminated SAM coated Si.

On the contrary, in-situ prepared samples were amorphous at the time of deposition, and further annealing treatments up to 1000°C did not produce a crystalline phase. This behavior is in fact consistent with the zirconium sulfate powder obtained from the same reaction solution hydrolyzed at 80°C, which did not show crystalline phases after a 1000°C treatment. Clearly, there exist chemical reactions involved in the in-situ prepared process unlike the physically deposited spin coating.

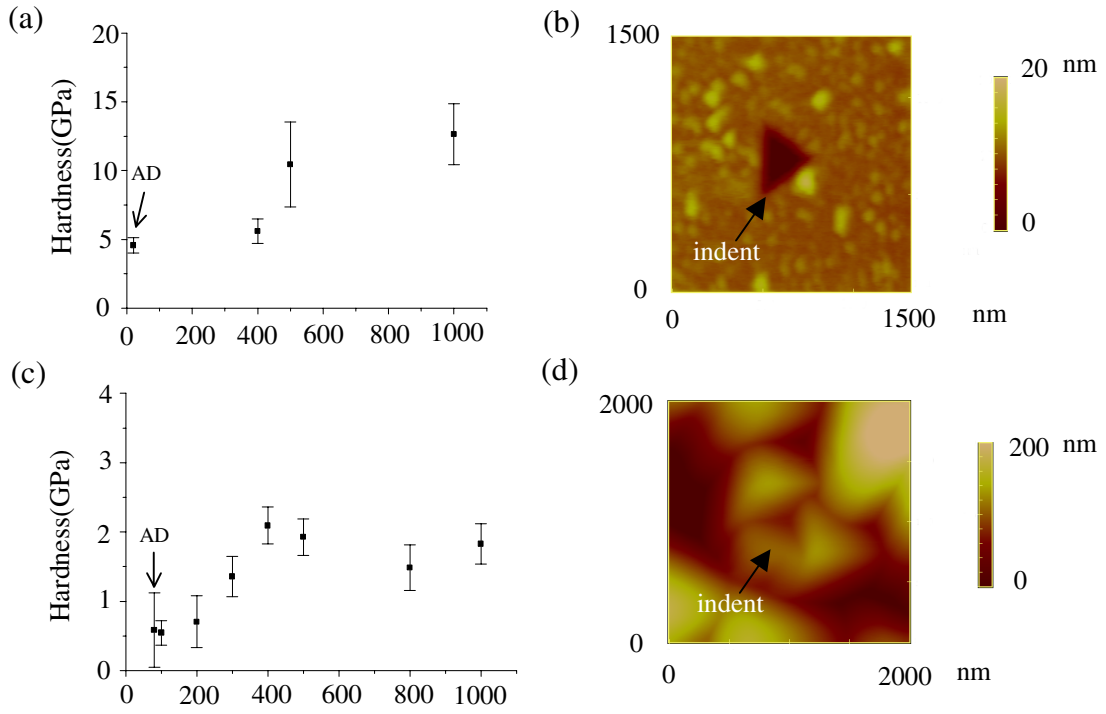

Figure 3. (a), (b): spin-coated sample using 3-*m* zirconium sulfate solution on -PO_3H_2 terminated SAM coated Si. (c),(d): in-situ solution sample prepared in 0.01-*m* zirconium sulfate solution heated at 80°C using -PO_3H_2 terminated SAM coated Si substrate. (a), (c): hardness evolution with temperature (AD: as-deposited sample). (b), (d): AFM images after indentation.

Hardness of the coating was measured using a nanoindenter. For the spin-coated films prepared from the $Zr(SO_4)_2{\cdot}4H_2O$ solution, the hardness values were almost constant for the samples treated until 400°C (Fig. 3a). These values increased at 500˚C due to the structural change (from crystalline zirconium sulfate to amorphous) at this temperature. It is noted that the crystalline ZrO_2 was not formed at this point. Hardness values, however, did not show much change after the formation of a crystalline ZrO_2. In-situ solution prepared samples gave hardness value less than 1 GPa when annealed at temperatures below 300˚C (Fig. 3c). An increase in hardness was observed after 300˚C. At temperatures above 400˚C, no noticeable change in

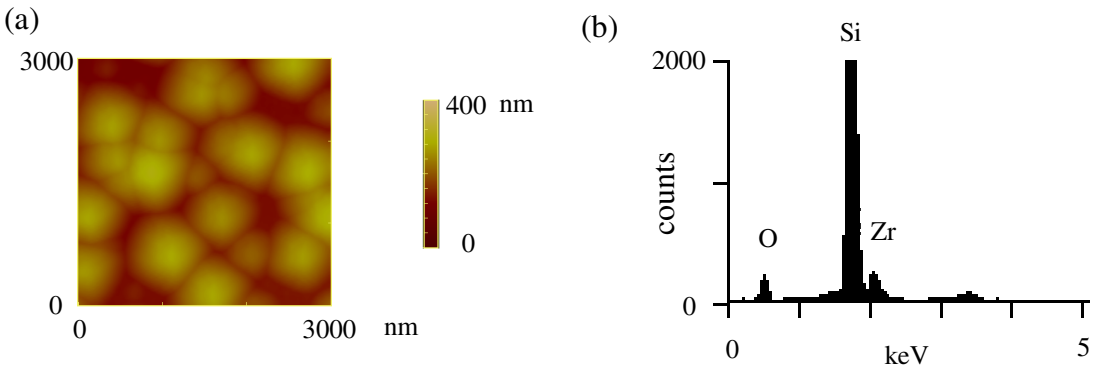

Figure 4. (a) AFM image, and (b) EDS result of in-situ solution prepared sample in 0.01-*m* zirconium sulfate solution heated at 80°C using -PO_3H_2 terminated SAM coated Si as a substrate (note on a Zr and O peak).

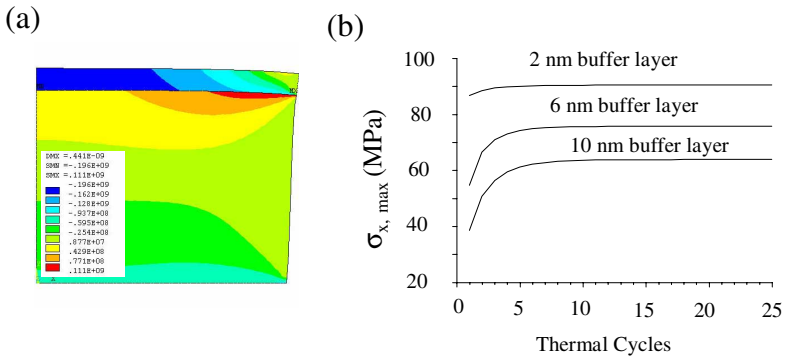

Figure 5. Stress development in a bilayer structure. (a) contour plot of σ_x when the bilayer structure was heated from 20°C to 200°C; (b) evolution of residual $\sigma_{x,\,max}$ with thermal cycles (20°C⇔ 200°C)

hardness was observed. Hardness values obtained by nanoindentation indicated that amorphous coating made by the in-situ solution process was rather soft.

Figure 4a shows an AFM image of the in-situ prepared sample. It shows an aggregation of particulates, each of which is around or less than 1-μm. EDS result showed clearly that the coating contained Zr and O (Fig. 4b), but as mentioned before, crystalline ZrO_2 was not formed when annealed at high temperatures. This phase evolution behavior is currently under investigation.

Numerical simulation was also employed to study the stress and strain development in the bilayer coating structure (ceramic/SAM). A simple 2-D model was established to study the stress distribution in the bilayer coating samples caused by a CTE (coefficient of thermal expansion) mismatch during heating/cooling cycles. This simulation was performed to assess the effect of the organic layer beneath the protective ceramic layer. Figure 5a was the contour plot of σ_x in bilayer structure when it was heated from 20°C to 200°C. Current modeling results indicated that residual $\sigma_{x,\,max}$ decreased monotonously with an increase of a buffer layer thickness (Fig. 5b). Therefore, an organic buffer layer between Si and ceramic film will greatly relieve the stresses developed in the ceramic layer. Further, the stresses are developed for longer time for the thicker buffer layer.

For a better understanding of the bilayer mechanics as well as to aid the aforementioned simulation work, mechanical property data of the SAM are needed. Due to the very thin nature of the SAM layer (one molecular thickness, Fig. 6a), however, its mechanical properties have not been well characterized. We used a nanoindentation technique to explore the mechanical properties of the SAM. Figure 6b shows a preliminary result on a load versus displacement curve for the -$SiCl_3$-terminated SAM whose thickness was ~8 nm, as measured by ellipsometry. Hardness of this SAM is ≈ 0.3 GPa, and elastic modulus is ≈ 52 GPa. This hardness is an acceptable range, while modulus data seem to be overestimated due to a substrate effect [16-18]. More systematic studies are needed to obtain a better understanding of mechanical behavior of the SAM.

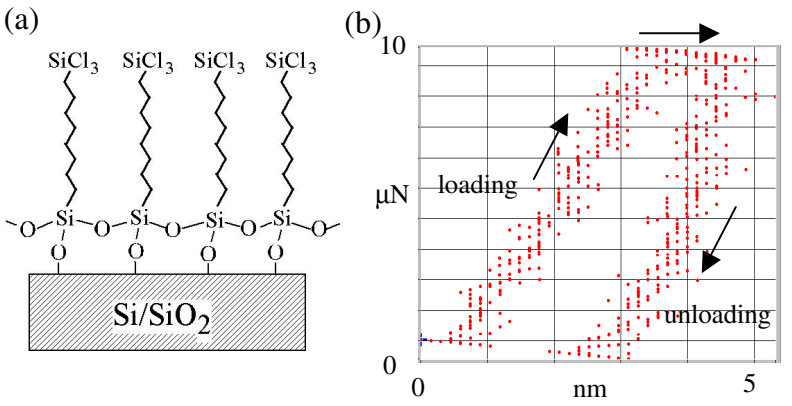

Figure 6. Characterization of the SAM layer: (a) schematic of -$SiCl_3$ terminated SAM; (b) nanoindentation test on -$SiCl_3$ terminated SAM coated Si (loading/unloading curve, max. load = 10 μN, max. depth = 5 nm).

CONCLUSIONS

Ceramic/SAM bilayer coatings were characterized using a variety of techniques such as XRD, AFM, SEM/EDS and nanoindentation. The spin-coated samples showed different features than those obtained from the in-situ solution prepared samples. XRD confirmed that the as-spin-coated sample was a crystalline zirconium sulfate that evolves to an amorphous phase at ~500°C followed by *t*- and *m*-ZrO_2 crystalline phases after 800˚C annealing. The in-situ prepared coating remained as an amorphous phase even after higher temperature annealing (up to 1000°C). In addition, this process is very sensitive to the pH of the precursor solution. The hardness of the amorphous coating that was prepared in situ in the precursor solution was much lower than that of the spin-coated ZrO_2 sample. Numerical simulation showed a benefit of the buffer layer in the bilayer structure, which gives a relief of CTE mismatch stress in the ceramic film.

ACKNOWLEDGMENTS

This work was funded by Infotonics Technology Center Inc. (US DOE Grant #: DE-FG02-02ER63410.A000) and partially supported by Integrated Electronics Engineering Center (IEEC) at State University of New York at Binghamton. The authors would also like to thank Prof. X. Wang and Mr. Y. Liu at Alfred University for helping with SEM/EDS work.

REFERENCES

1. T. A. Core, W. K. Tsang, and S. J. Sherman, Solid State Technol., **36** (10) 39-44 (1993).
2. T. Tsuchiya, Y. Kageyama, H. Funabashi, and J. Sakata, Sensors and Actuators A, **90**, 49-55 (2001).
3. F. Ayazi, J. Microelecromechanical Syst., **10** (2) 169-79 (2001).
4. K. Gilleo, IEEE Transactions on Components and Packaging Technologies **24** (2), 309-311 (2001).
5. N. Maluf, *An Introduction to Microelectromechanical Systems* (Artech House, Inc., Norwood, MA, 2000).
6. G. W. Goward, Mater. Sci. Tech., **2**, 194-200 (1986).
7. R. A. Miller, J. Therm. Spray Technol., **6** (1) 35-42 (1997).
8. D. I. Pantelis, P. Psyllaki, and N. Alexopoulos, Wear, **237** (2) 197-204 (2000).
9. S. Bahadur and C.-N. Yang, Wear, **196** (1-2) 156-63 (1996).
10. C.-P. Klages, M. Fryda, T. Matthée, L. Schäfer and H. Dimigen, Int. J. Refrac. Metals and Hard Mater., **16** (3) 171-76 (1998).
11. A. R. Bishop, R. G. Nuzzo, Curr. Opin. Col. Int. Sci., **1**, 127-136 (1996).
12. A. Ulman, Chem. Rev., **96**, 1533-1554 (1996).
13. S. W. Keller, H.-N. Kim, T. E. Mallouk, J. Am. Chem. Soc., **116**, 8817-8818 (1994).
14. G. M. Whitesides, Sci. Amer. Sept., 146-149 (1995).
15. W. C. Oliver and G. M. Pharr, J. Mater. Res., **7** (6), (1992).
16. R. Saha and W. D. Nix, Acta Materialia **50**, 23–38, (2002).
17. N. G. Chechenin, J. Bottiger, and J. P. Krog. Thin Solid Films **261** (1-2), 219-227 (1995).
18. M. F. Doerner, D. S. Gardner, W. D. Nix, J Mater Res **1**, (1986).